Armadillo Repeat Only Proteins Are Required for the Function of Plant CNGC Channels.

Ivan Kulich[1,2]*, Denisa Oulehlová[3,6], Dmitrii Vladimirtsev[1], Minxia Zou[1], Edita Lileikyte[2], Alexey Bondar[2], Katarína Kulichová[2], Martin Janda[4], Oksana Iakovenko[4], Michaela Neubergerová[3,6], Tanja Studtrucker[5], Roman Pleskot[3], Petra Dietrich[5], Matyáš Fendrych[3], Jiří Friml[1]*

Affiliations:

[1] Institute of Science and Technology Austria (ISTA), Austria
[2] Institute of Plant Molecular Biology (IPMB) of Czech Academy of Sciences, Czechia
[3] Institute of Experimental Botany (IEB), Czech Academy of Sciences, Czechia
[4] Faculty of Science, University of South Bohemia, Czechia
[5] Friedrich-Alexander-Universität Erlangen-Nürnberg, Molecular Plant Physiology, Erlangen, Germany
[6] Faculty of Science, Charles University, Czechia

*correspondence: Ivan Kulich: ivan.kulich@umbr.cas.cz; Jiri Friml: jiri.friml@ist.ac.at

Abstract

Plant cells respond to a wide range of stimuli through intracellular calcium (Ca^{2+}) signaling. Cyclic nucleotide-gated channels (CNGCs) are a major class of plant Ca^{2+} channels, with 20 homologs in *Arabidopsis*. These tetrameric plasma membrane proteins act downstream of diverse signals, such as phytohormones, extracellular damage, cell wall integrity or temperature. Here, we identify a class of plant-specific proteins, Armadillo Repeat Only (ARO), as essential regulators of possibly all plant CNGCs. Abrogation of functional sporophytic AROs results in a phenotypic pattern strongly reminiscent of CNGC dysfunction, including defects in root gravitropism, root hair growth and morphology, stomatal movement, and responses to extracellular ATP and the phytohormone auxin. *aro2/3/4* mutants are fully resistant to the toxic effects caused by overexpression of CNGCs. AROs colocalize and physically interact with multiple CNGCs and modulate CNGC-dependent currents in *Xenopus* oocytes. Structural modeling and site-directed mutagenesis reveal AROs tetramer formation surrounding the CNGC channel, interacting via its IQ domain. Taken together, plant CNGC channels don't act alone, but in a larger complex - channelosome, first of a kind in plants.

Introduction

Signaling mediated by cytoplasmic Ca^{2+} is an indispensable mechanism conserved across eukaryotes. Plants use Ca^{2+} signaling to sense and respond to external and internal stimuli. Cyclic nucleotide gated channels (CNGCs) are a class of tetrameric ion channels, which are essential for a broad spectrum of processes including hormonal responses, stomatal movements[1,2], tip growth[3,4], responses to pathogen and damage-associated molecular patterns (PAMPs, DAMPs, respectively[5–7]). Responses to specific stimuli usually require a specific channel, with CNGC2 being downstream of extracellular ATP (eATP) and plant elicitor peptides (PEP) response, CNGC14 downstream of phytohormone auxin, CNGC12 downstream of flagellin peptide FLG22, etc.[5,7,8].

Although numerous pathways are known to involve CNGCs, their exact operational mechanisms remain unclear. In heterologous systems, CNGCs exhibit hyperpolarization-activated conductance, suggesting voltage gating. However, other studies indicate ligand gating, wherein activation by cAMP or cGMP may be voltage-dependent or independent[4,6,9–11]. Calmodulin gating was also implied. On the top of the voltage dependency, calmodulin, which binds constitutively to the CNGCs is the key factor in CNGC2-4 heterotetramer gating[12]. Multiple studies highlight phosphorylation as the mechanism of CNGC regulation *in planta*, however, it is unclear whether and how this contributes to the gating mechanism[2,12,13]. To summarize, there is a lack of clear consensus on the CNGC gating, which signifies a deeper lack of understanding of the CNGC channel biology.

Armadillo Repeat Only (ARO proteins) have been so far unsuspected players, which may hold the key to our understanding of CNGC channel function. AROs are a class of 4 proteins which contain two sets of ARM repeats separated by an unstructured linker region. Initially ARO1 was described to be essential for the pollen tube growth[14]. Sporophytic AROs – ARO2,3 and 4 have been shown to be essential for trichome and root hair growth in the *Arabidopsis* sporophyte[15]. Like in the pollen tubes, *aro2/3/4* mutant root hair either abort or burst soon after bulging – similarly like *cngc6/9/14* triple mutant[3]. This was linked to the inability to spatially restrict ROP GTPase activity and to the loss of polarity. Importantly, all AROs are functionally redundant. ARO from *Marchantia polymorpha* complemented Arabidopsis *aro2/3/4* mutant phenotypes demonstrating large degree of conservation of its function in land plants[15].

Here we provide the evidence, that the major cause of the *aro2/3/4* mutant phenotypes is caused by lack of the functionality of multiple CNGC channels and establish AROs as interactors and indispensable accessory proteins for CNGC function.

Results

aro2/3/4 mutants phenocopy higher order *cngc* mutants

The most notable phenotype of the *aro2/3/4* triple mutant is the bursting of trichomes and root hairs (Fig. 1A), a phenomenon previously described[15]. In addition to this phenotype, *aro2/3/4* mutant roots exhibit enhanced waving when grown at a 45° angle (Fig. 1A, B). This phenotype closely resembles that of the *cngc14-2* mutant (Fig. 1A, B) and the *cngc6/9/14* triple mutant, which also display both root waving and root hair bursting phenotype[3] (Fig 1A,B).

Given that the increased waving in the *cngc14-2* mutant results from the delayed response to gravitropic stimuli[8], we measured gravitropic bending in both *cngc14-2* and *aro2/3/4* mutants. Both mutants exhibited a similar initial delay in gravitropic bending (Fig. 1C). A comparable phenotype was observed in the *aro2/4* double mutant (Fig. S1A), consistent with the expression of ARO3 being restricted to the differentiation zone[15]. Higher temporal resolution observations of the root gravitropic response revealed that the most pronounced defect occurred approximately within one hour after gravistimulation (Fig. S1B; Supplementary Movie 1).

Using a fluorescent dye to monitor apoplastic pH (Fluorescein-5-(and-6)-Sulfonic Acid, Trisodium Salt; FS)[16], we found that the *aro2/3/4* mutants failed to alkalinize the lower side of the root during gravitropic bending (Fig. 1D, E; Supplementary Movie 2). This defect mirrors previously reported observations in *afb1* and *cngc14* mutants[17–20]. Similarly, auxin induced membrane depolarization was absent in *aro2/3/4* mutants (Fig. S1C). Importantly, auxin transport and nuclear auxin response during gravitropism remained functional, as judged based on the experiments using the R2D2 nuclear auxin response reporters (Fig. S1D), indicating a specific defect in the rapid auxin response[21].

Next, we investigated the auxin-induced rapid root growth inhibition using a microfluidic setup[18]. This analysis revealed that *aro2/3/4* mutants lack auxin-induced rapid root growth inhibition entirely (Fig. 1F). Taken together, the waving and gravitropic bending phenotypes in *aro2/3/4* can be attributed to the absence of rapid auxin responses mediated by CNGC14, while the lack of root hair development may reflect a combined effect of CNGC6, 9, and 14.

Another key phenotype in *cngc* mutants is a defective stomatal movement, as CNGC-induced Ca^{2+} transients are essential for stomatal closure[1,2]. Similarly, the *aro2/3/4* triple mutant shows a severe defect in stomatal closure (Fig. 1G, H), phenocopying the *cngc5/6/9/12* quadruple mutant[1].

In summary, the phenotypes observed in *aro2/3/4* mutants, including defects in root hair growth, gravitropic bending, and stomatal movements, are similar to impairments in calcium-related pathways; specifically, those found in various *cngc* mutants.

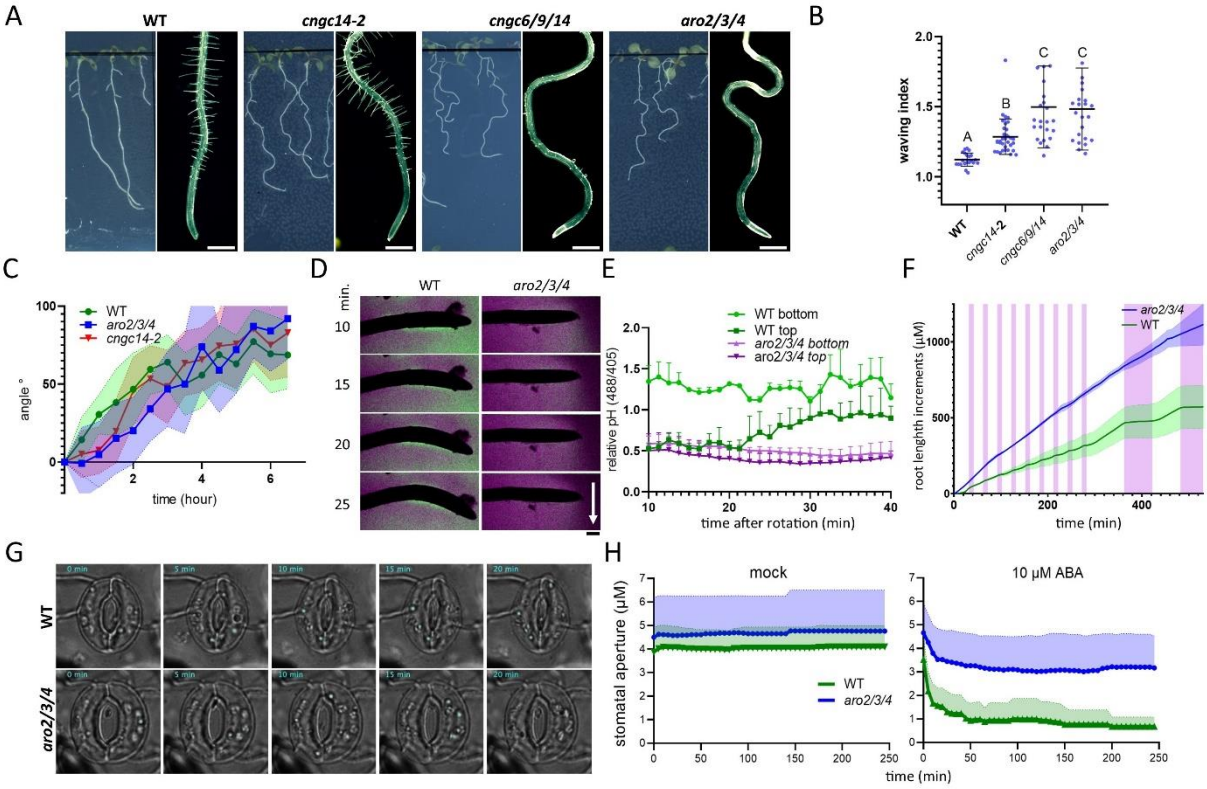

Figure 1: *aro2/3/4* mutants phenocopy higher order *cngc* mutants.

(A) Representative images depict root waving phenotype on tilted plates (left panel) and root hair growth phenotype (right panel) of *aro2/3/4* in comparison with *cngc14-2* and *cngc6/9/14* triple mutants. 7 day old seedlings. Bars=500µm.

(B) Quantification of the root waving shown as the waving index. Each measurement (n>20) represents an individual root grown on an 45°angle. Error bars = SD.

(C) Root gravitropic bending of *aro2/3/4* and *cngc14-2* mutants. 14 plants per genotype were evaluated. Similar results were obtained >3 times. Colored areas = SD.

(D) Apoplastic pH profile of the *aro2/3/4* mutants and WT in the course of the root gravitropic bending, where green halo represents alkaline shift and magenta halo represents acidic shift and gravitropic vector is depicted by an arrow. Whole movie - Supplementary Movie 2. Bar=50µm.

(E) Quantification of the pH shifts from (D) on 3 roots per genotype. Two similar replicas were generated. Error bars = SD.

(F) Kinetics of the root growth inhibition upon auxin treatment. Magenta stripes represent time windows with 10nM IAA. Growth increments were averaged from 2 plants; similar experiments were obtained >3 times. Colored areas = SD Pink stripes represent the time windows with the treatment

(H) Representative stomatal aperture upon 10µM ABA treatment.

(H) Quantification of the stomatal aperture after ABA treatment. 10 stomata per genotype were measured.

Colored areas = SD.

CNGC-mediated Ca^{2+} transients are absent in the *aro2/3/4* triple mutant

To further investigate Ca^{2+} homeostasis of the *aro2/3/4* triple mutant, we crossed it to the intracellular Ca^{2+} reporter GCaMP3.0[22]. Microfluidic experiments revealed a complete absence of the IAA-induced Ca^{2+} transient in *aro2/3/4* mutants (Fig. 2A; Supplementary Movie 3). eATP, which triggers CNGC2- or CNGC6-dependent Ca^{2+} transients[7,23], also failed to elicit a response in *aro2/3/4* triple mutant roots (Fig. 2B). Similarly, the PEP1 peptide, previously described as an activator of the CNGC2 channel[6], did not trigger Ca^{2+} transients in *aro2/3/4* mutants (Fig. S1E).

To determine whether the stomatal defects in *aro2/3/4* are also linked to disrupted Ca^{2+} signaling, we exposed seven-day-old cotyledons to drought stress. In wild type (WT) plants, drought stress induced Ca^{2+} signaling in stomata, whereas these transients were reduced in the *aro2/3/4* triple mutants (Fig. 2C; Supplementary Movie 4).

In contrast, *aro2/3/4* mutants retained Ca^{2+} transients mediated by different Ca^{2+} channels such as GLR3.3 and 3.6[22], which are activated by glutamate (Fig. 2D), as well as MCA1-dependent Ca^{2+} transients elicited by plasma membrane (PM) stretching[24] (Fig. 2E).

In summary, all tested CNGC-dependent Ca^{2+} signaling processes were absent in *aro2/3/4* mutants, while CNGC-independent Ca^{2+} transients remained intact (Fig. 2F). These confined stimulus-specific Ca^{2+} response phenotypes show that AROs specifically target CNGC-dependent pathways and may be intimately linked with their functions.

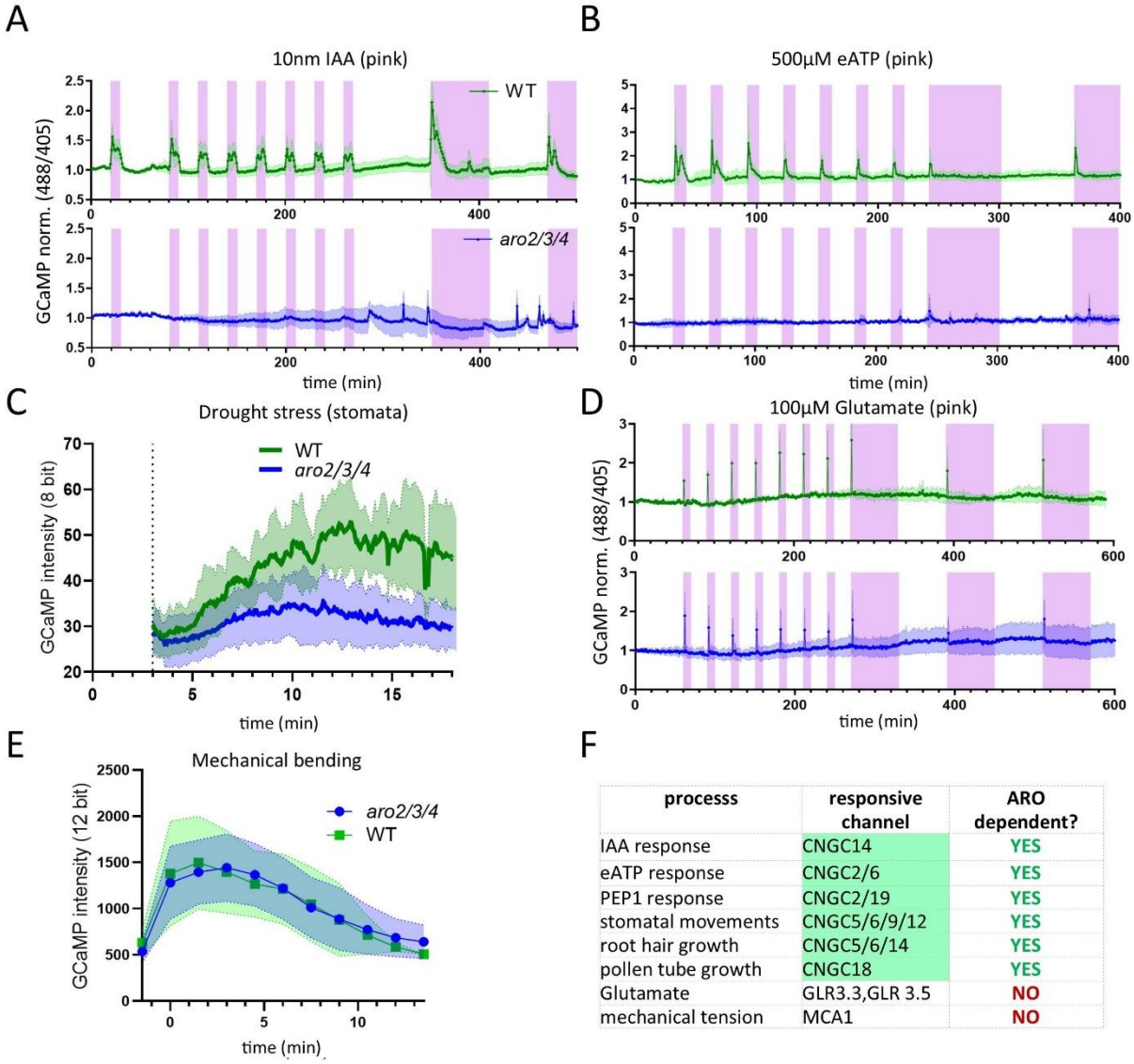

F

processs	responsive channel	ARO dependent?
IAA response	CNGC14	YES
eATP response	CNGC2/6	YES
PEP1 response	CNGC2/19	YES
stomatal movements	CNGC5/6/9/12	YES
root hair growth	CNGC5/6/14	YES
pollen tube growth	CNGC18	YES
Glutamate	GLR3.3,GLR 3.5	NO
mechanical tension	MCA1	NO

Figure 2: *aro2/3/4* mutants fail to generate CNGC dependent Ca^{2+} transients

(A) 10nM IAA treatment fails to induce Ca^{2+} transients in *aro2/3/4* mutants. Pink stripes represent the time windows with the treatment. Average of 3 roots. Two more similar replicas were generated. CGaMP intensity was normalized as follows: ($GCAMP^{ex488}/GCaMP^{ex405}$)/baseline (avg of t1-t30).

(B) 500µM eATP treatment fails to generate Ca^{2+} transients in *aro2/3/4* mutants. Four plants per treatment were measured and experiment was repeated twice.

(C) Guard cell GCAMP intensity upon drought stress. 16 guard cells were imaged. Experiment was repeated 3 times.

(D) 100µM glutamate treatment induces comparable Ca^{2+} transients in both *aro2/3/4* and WT. Pink stripes represent the time windows with the treatment. 3 plants per genotype were evaluated. Similar results were observed 3 times.

(E) Mechanical bending induces Ca^{2+} transient on the convex side of the root in both *aro2/3/4* and WT plants. 6 plants were measured. Experiment was repeated two times.

(F) Summary of the multiple responses and phenotypes of *aro2/3/4* mutants along with responsible Ca^{2+} channels. Colored areas = SD Pink stripes represent the time windows with the treatment.

AROs interact with and stabilize CNGCs

Due to functional redundancy between AROs and their involvement in functionality of multiple CNGC channels, we selected ARO2, CNGC14 and CNGC2 as representative proteins. We transformed *aro2/3/4* triple mutants with CNGC14-mCHERRY (mCH) or CNGC14-GFP under the native CNGC14 promoter. We then complemented the CNGC14-mCH-transformed plants with ARO2-mCIT, also driven by its native promoter. CNGC14-mCH colocalized with ARO2-mCIT at the PM, including the shank region of root hairs. Both, ARO2-mCIT CNGC14-mCH co-localized in the root epidermis, mainly in the shank of the growing root hair (Fig. 3A, Supplementary Movie 5). Importantly, plasma membrane localization of ARO2-mCIT was completely lost when observed in *cngc6/9/14* mutant. This demonstrates that CNGCs and AROs form a complex *in vivo*.

Consistent with these observations, ARO2 interacted with both CNGC14 and CNGC2 when transiently expressed in *N. benthamiana* under ubiquitin promoters, as demonstrated by fluorescence lifetime (FRET-FLIM) experiments (Fig. 3B). Notably, in *N. benthamiana* samples co-transformed with UBQp-ARO2-mCH, the signal of UBQp-CNGC14-GFP was consistently stronger compared to UBQp-CNGC14-GFP co-transformed with UBQp-mCH. To ensure that the FRET-FLIM results were not influenced by protein levels, we included a negative control using 6xHIS-ARO2 without a fluorescent tag (Fig. 3B).

To determine whether this stabilization effect was specific to CNGCs, we tested if ARO2 could stabilize other, functionally unrelated PM proteins. ARO2 had the most significant stabilizing effect on CNGC14, followed by CNGC2, but it had no significant impact on other unrelated proteins (Fig. 3C, D). Supporting these findings, our IP-MS analysis using ARO2p identified peptides corresponding to multiple CNGCs, including CNGC1, 5, 6, 8, 9, 15, 16, and 17, with no peptides detected in the negative control (PBR-GFP-TID-HA, where PBR corresponds to a polybasic region that recruits GFP to the PM) (Fig. S2).

In summary, AROs interact with multiple CNGCs, possibly forming a larger functional protein complex.

The Critical role of AROs in CNGC function extends beyond stabilization

Next, we tested whether ARO-dependent stabilization of CNGCs can explain the *aro2/3/4* phenotypes. We observed CNGC14-GFP under its native promoter in both *aro2/3/4* and WT plants, selecting several lines with comparable CNGC14-GFP signal intensity. In both genotypes, CNGC14-GFP localized consistently to punctate structures on the PM, with no visible differences (Fig. 3E). Despite this comparable protein abundance and localization, *aro2/3/4* mutants expressing CNGC14-GFP continued to develop the characteristic phenotypic deviations, such as increased waving (Fig. 3F) and delayed root gravitropic bending (Fig. 3G) This observation strongly suggests that, while ARO stabilizes CNGC14 upon overexpression in tobacco leaves, the mutant phenotypes in *aro2/3/4* are not due to changes in CNGC amounts at the PM.

In line with CNGC14 function, expressing CNGC14-GFP under its native promoter in WT plants led to significantly shorter roots, suggesting a slight toxicity of the CNGC14-GFP construct. However, this effect was absent in *aro2/3/4* mutants, which showed no significant impact on root length (Fig. S3A-C). Similarly, overexpression of CNGC2-mCit under the ubiquitin promoter caused dwarfism in WT plants,

whereas no such effect was observed in *aro2/3/4* mutants (Fig. S3D,E). This further demonstrates that

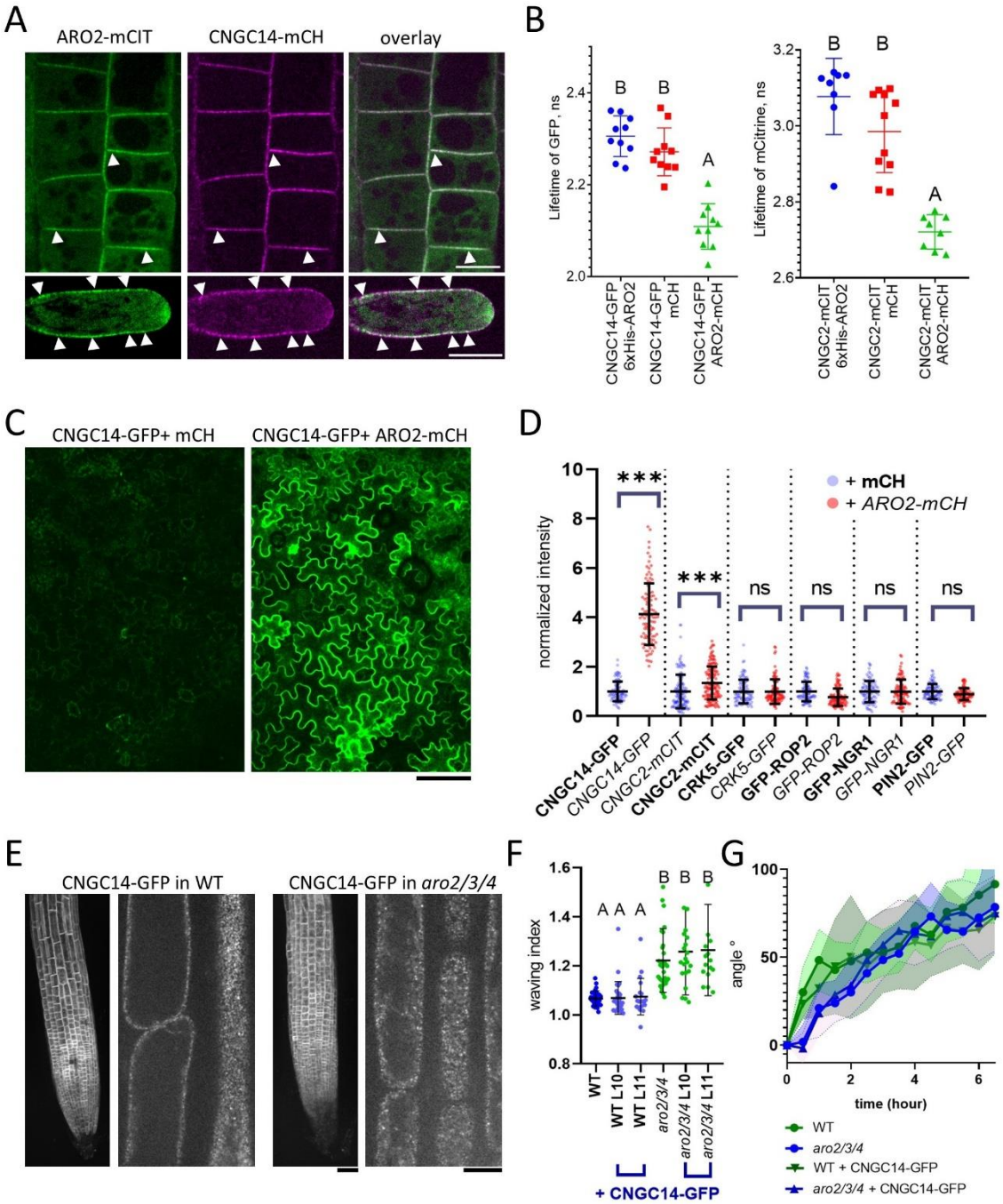

Figure 3| ARO colocalizes, interacts with and stabilizes CNGC channels

(A) Representative images depict colocalization of ARO2-mCIT and CNGC14-mCH in complemented *aro2/3/4* mutants. Note the overlapping dots in the growing root hair and meristem (white arrowheads). Video of the root hair growth – supplementary movie 5. Bar = 10 µm

(B) FRET-FLIM results performed in *N.benthamiana* show positive interaction result for both CNGC14-ARO2 and CNGC2-ARO2 pairs. Letters depict significantly different datasets with p-value <0.0001 (one-way ANOVA). Each measurement represents inidvidual cell (n=10)

(C) Representative image of the stabilization effect of mCH and ARO2-mCH on the CNGC14 abundance, when expressed under UBQ10 promoter in *N.benthamiana.* Bar=100 µm

(D) Quantification of the ARO dependent stabilization effect on CNGCs and different other PM proteins shows specificity for the CNGC channels. Note that CNGC2 stabilization effect was much weaker due to already strong signal without ARO. Two measurements per cell were performed with 50 cells per genotype. Normalization was done so to that the cells

transfected with free mCHERRY = 1. Asterisks depict significantly different datasets with p-value <0.0001 (one-way ANOVA)

(E) CNGC14-GFP under its native promoter displays similar localization in *aro2/3/4* mutant and WT. Left – overview of the whole root, right – cortical section of the PM displaying similar punctate pattern. Bars=50µm (left), 10µm (right)

(F) *aro2/3/4* mutant lines expressing comparable amounts of CNGC14-GFP still retain all the *aro2/3/4* mutant phenotypes, demonstrated here as a root waving phenotype. Each dot represents a single root (n>15). Different letters denote significantly different results with p < 0.0002 (one-way ANOVA).

(G) *aro2/3/4* mutant lines expressing comparable amounts of CNGC14-GFP still retain the gravitropic bending phenotypes 14 roots per genotype were evaluated. Data from two individual lines were pooled together for improved readability.

the channels are non-functional in the *aro2/3/4* background, even though CNGC2 subcellular localization remained unaffected.

In summary, ARO proteins are direct interactors of CNGCs that are essential for CNGC functionality *in planta*.

AROs directly modulate CNGC functionality in *Xenopus* oocytes

The similar localization of CNGCs in WT and *aro2/3/4* mutants rules out that AROs impact on CNGC functionality is due to their effect on the channel trafficking. To determine whether AROs can directly modulate CNGC activity, we microinjected cRNAs encoding VN-ARO2 and CNGC14-VC (where VN and VC refer to split mVenus parts) into *Xenopus* oocytes. While water-injected or VN-ARO2-injected oocytes showed minimal or no currents, oocytes expressing CNGC14-VC displayed hyperpolarization-activated inward currents (Fig. 4A). When ARO2 was co-injected, overall current amplitudes were reduced, along with a time- and voltage-dependent current inhibition (Fig. 4A, B).

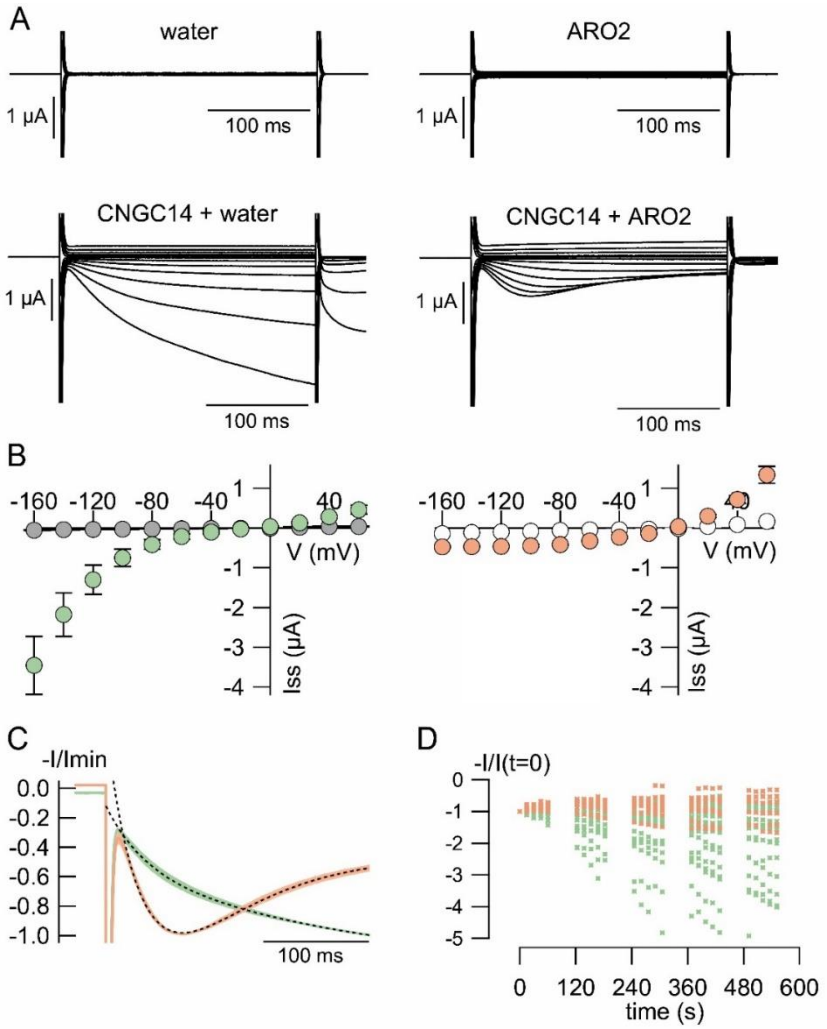

Figure 4| ARO2 facilitates opening of CNGC14 while inducing time- and voltage-dependent inhibition

(A) Representative current responses of individual oocytes injected with water or cRNA of *VN-ARO2* alone, *CNGC14-VC* or *CNGC14-VC* together with *VN-ARO2*. Current traces were obtained in the presence of 30 mM $CaCl_2$, 1 mM KCl, pH 7.4, at test voltages ranging from +60 mV to -160 mV in 20 mV decrements.

(B) Mean steady-state current voltage relations obtained from current traces as shown in (A), for oocytes injected with water (grey, n=4) or *CNGC14-VC* (green, n=19) or *VN-ARO2* (white, n=10) or *CNGC14-VC* plus *VN-ARO2* (orange, n=15).

(C) Comparison of average CNGC14 kinetics upon a voltage step from -30 mV to -120 mV in the absence (green, n=21) or presence (orange, n=8) of VN-ARO2, 8 min after impalement. Each current trace was normalized to its minimum value, and data represent mean ± s.e.m. depicted as 75% color intensity area. Kinetics could be described by double exponential fits (dotted lines).

(D) Time-dependence of CNGC14 inward currents recorded at -140 mV in the absence (green, n=22) or presence (orange, n=9) of VN-ARO2. Maximal negative (not steady-state) current amplitudes were normalized to the value after impalement (t=0).

Interestingly, despite these inhibitory effects, the presence of ARO2 also accelerated the activation kinetics of CNGC14, in accordance with a facilitation of channel opening (Fig. 4C). This behavior suggests that ARO proteins both enhance and restrict Ca^{2+} entry into the cells. Notably, oocytes injected with both VN-ARO2 and CNGC14-VC, but not with VN-ARO2 alone, appeared softer and more fragile, limiting the scope of analysis. The impairment of oocyte integrity may reflect stress triggered by the ARO-CNGC combination and suggests the presence of a functional channel complex.

In summary, ARO alone can influence CNGC14 activity in *Xenopus* oocytes. The observed effects substantially deviate from all other regulations observed so far, which either enhanced or reduced current amplitudes but did not act on a comparable time scale. Further observations and additional contextual information are needed to interpret these findings in the context of plant cell function.

CNGCs interact with AROs via their IQ domain, forming larger molecular complex

Knowing that AROs directly interact with and modulate CNGC activity, we performed structural modeling of the CNGC14 tetramer in complex with ARO2 AlphaFold2[25,26] (Fig. 5 and Fig. S4) to test the possibility that AROs form a complex with CNGCs. AlphaFold2 confidently predicts a double tetramer complex (Fig. 5A), where each CNGC14 monomer recruits ARO via its IQ domain (Fig. 5B), which is the same region binding calmodulins[27]. The model is consistent with the findings from[15] where N-terminal basic residues of ARO2 interact with the plasma membrane (Fig. 5C).

To test involvement of the IQ domain in ARO-CNGC interaction, we repeated FRET-FLIM of ARO2 and CNGC14 with or without IQ domain ($CNGC14^{\Delta IQ}$) (Fig. 5D, E). Removal of IQ domain returned the fluorescence lifetime to the levels of the negative controls (Fig. 5E). This confirms that the IQ domain is essential for the interaction between ARO2 and CNGC14, supporting the predictions made by Alphafold2.

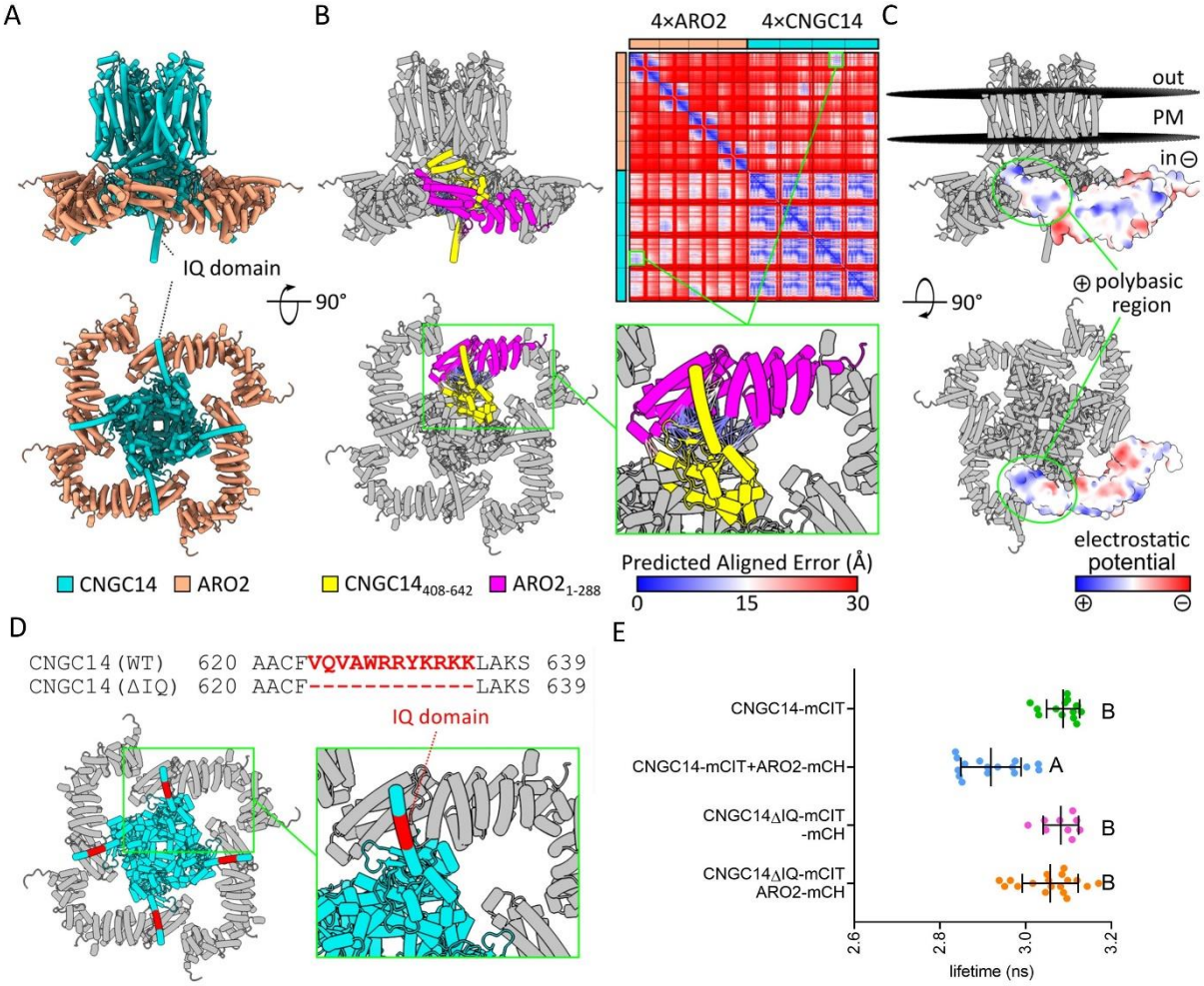

Figure 5| Four ARO2 proteins form the complex with the CNGC14 tetramer

(A) AlphaFold2 prediction of the ARO2-CNGC14 complex. Parts predicted with the low pLDDT score were excluded from the visualization (see Methods and Fig. S5).

(B) C-terminal part of CNGC14 (IQ domain) and the N-terminus of ARO2 forming the interaction interface are highlighted in yellow and magenta. The Predicted Aligned Error (PAE) plot shows AlphaFold2 is confident about this interaction. The zoom-in image highlights contacts under 8 Å between these regions. Lines are colored according to the PAE values, with most contacts showing high confidence.

(C) The PPM3.0 positioning of the ARO2-CNGC14 complex in the membrane. Electrostatic potential mapped on one of the ARO2 subunits shows the N-terminal polybasic region, previously described to mediate the interaction with anionic phospholipids of the PM (Kulich et al., 2020) is oriented towards the membrane and thus enabling its interaction with negatively charged phospholipids.

(D) Depiction of the IQ domain (red) and its deletion (ΔIQ)

(E) FRET-FLIM measurement of the CNGC-ARO interaction showing IQ domain is essential for the CNGC binding to ARO. Letters depict significantly different datasets with p-value <0.0001 (one-way ANOVA). Experiment was repeated 3 times.

Discussion

AROs – new kids on the CNGC block

In this study, we identify the Armadillo Repeat Only (ARO) protein family as essential for the functionality of a wide range of CNGC channels. After decades of enigmatic and often contradictory results on CNGC regulation[10,28], knowing that there is an essential and conserved functional element will be essential for learning how CNGCs actually operate.

Given that AROs are highly conserved across land plants—for instance, ARO from *Marchantia polymorpha* is functional in *Arabidopsis*[15]—they likely represent a conserved mechanism necessary for

275 the operation of multiple, perhaps all, plant CNGCs. This is further supported by the identification of
276 several CNGCs as ARO2 interactors. The direct interaction between AROs and multiple CNGCs, along
277 with the impact of AROs on Ca^{2+} transients, underscores their essential role in CNGC functionality.
278 Furthermore, the effect of AROs on CNGC channel activity in *Xenopus* oocytes demonstrates their direct
279 involvement in channel operation. Stress, evoked by simultaneous microinjection of AROs and CNGCs
280 implies its involvement in channel activity far more potent than modulations such as phosphorylation.

281 While this study primarily focuses on sporophytic AROs, similar roles are expected for the gametophytic
282 ARO1. Notably, ARO1 driven by ARO2 promoter can complement *aro2/3/4* mutant phenotypes[15], and
283 the *aro1* mutant exhibits defective pollen tubes characterized by bloating and bursting[14]. This
284 phenotype is much stronger than *cngc18* mutant phenotype[4], implying additional roles of remaining
285 CNGC channels.

286 Analysis of AROs brings further implications for the role of CNGC2 in the immune system. The *cngc2* is
287 a dwarf mutant which shows a lesion mimic phenotype[29,30] (plant equivalent of autoimmune disease).
288 In contrast, *aro2/3/4* mutants have WT size, if cultivated properly. In *aro2/3/4* mutants, CNGC2 is still
289 present, although channel is not functional, demonstrating that CNGC2 presence, not functionality, is
290 important for *cngc2* lesion mimic and dwarf phenotypes, thus CNGC2 integrity is probably guarded by
291 plants immune system. Further studying *aro2/3/4* mutants may bring a clear distinction between
292 immunity-related and signaling roles of CNGC2 and maybe also other CNGCs.

293 **ROP GTPases and Ca^{2+}**

294 Previously, we demonstrated that AROs are essential for the ROP GTPase cycle[15]. However, our current
295 findings reveal that most *aro2/3/4* mutant phenotypes can, in fact, be attributed to the absence of
296 CNGC activity. This novel discovery suggests that the regulation of the ROP cycle by AROs is likely
297 indirect and mediated through Ca^{2+} signaling. If this hypothesis holds true, ROP2, which we previously
298 found to be mislocalized in the *aro2/3/4* mutant, should also be mislocalized in the *cngc6/9/14* mutant.
299 This is indeed what we observed (Fig. S5), supporting this notion. While the precise mechanism
300 underlying this mislocalization remains unclear, it opens the door to several hypotheses. One potential
301 explanation involves REN1, a ROP GTPase-activating protein that is absent from the PM in the *aro2/3/4*
302 mutant[15]. We hypothesize that its membrane localization may be regulated by Ca^{2+}. Intriguingly, REN1
303 exhibits oscillatory behavior at the pollen tube tip [31] with a frequency and phase shift matching those
304 of Ca^{2+} oscillations[32]. This alignment raises the possibility that on the top of the direct recruitment,
305 AROs regulate the ROP cycle indirectly through their effects on Ca^{2+} homeostasis. Further research will
306 be required to unravel the precise connections between AROs, CNGCs, and the ROP cycle.

307 **What are plant Channelosomes?**

308 While it is clear that AROs are involved in CNGC channel functionality, exact molecular mechanism
309 remains to be elucidated. ARM repeats are common protein-protein interaction motifs across
310 eukayotes. This raises a possibility that CNGC channels operate in larger protein complexes. Such
311 complexes would be more stable and have increased lifetime at the PM, explaining the ARO induced
312 CNGC stabilization. Since AROs interact with CNGCs via their IQ motif, stability and operation of such
313 complex may be modulated by competitive binding of calmodulins, which bind to the same region[27,33].

314 The idea of a larger molecular complex named channelosome is not new to the metazoan literature[34]
315 and is highly studied in the neurons. Here, Ca^{2+} channels are docked and regulated with proteins such
316 as ankyrins, which are required for proper localization of channel clustering and localization in the
317 axons, RACK1 (receptor for activated C kinase 1), which is a scaffold protein recruiting multitude of
318 signaling proteins to the channels[34]. In contrast with metazoans, channelosomes have never been

319 described in plants[28]. Being essential for their function, AROs may represent the first universal adaptor
320 ever described for plant CNGCs, foreseeing an era of plant channelosomes.

321 **Materials and Methods**

322 **Plant growth and conditions**

323 All *Arabidopsis* mutants and transgenic lines which were used in this project are in the Columbia-0 (Col-
324 0) background. *aro2/3/4* and *aro2/4* represent T-DNA insertional lines described previously[15]. *cngc14-*
325 2 were obtained from[8] and *cngc6/9/14* were obtained from[3]. *aro2/3/4* plants were crossed into the
326 plants expressing GCAMP3 obtained from[22]. WT expressing GCAMP3 was obtained as a sister plant
327 from the cross with *aro2/3/4* displaying similar signal intensity. *aro2/4* was crossed into R2D2
328 background[35] and verified by genotyping as previously[15]. Seeds were sterilized overnight using chlorine
329 gas and sown on solid agarose medium consisting of half-strength Murashige and Skoog medium with
330 or without B5 vitamins (Duchefa M0231) (with 1% sucrose (AM+) and 0.8% phyto agar, adjusted to pH
331 5.9. The sown seeds were stratified at 4 °C for 2 days, then grown vertically at 21 °C under a 16-hour
332 light/8-hour dark cycle.

333 **Plant treatments**

334 Treatments with ATP (Thermo Scientific R0441), IAA (Duchefa I0901), glutamate (Sigma; PHR2634-1G)
335 were performed in the microfluidic setup with equivalent amount of solvent added to the mock
336 control. PEP1 peptide (ATKVKAKQRGKEKVSSGRPGQHN; Chinese Peptide Co., LTD.) was used for a
337 direct treatment without microfluidics.

338 **Gravitropic and mechanical root bending assays**

339 Gravitropic bending experiments were conducted using a vertically oriented scanner setup. Four-day-
340 old seedlings were transferred to a fresh solid agarose medium plate, with roots aligned to maintain a
341 straight orientation. Images were captured at 30-minute intervals and registered using the Fiji StackReg
342 plugin[36]. Root tracking and angle increment calculations were performed manually in Microsoft Excel.
343 Mechanical bending was performed by positioning the root on a microscopy slide in a droplet of
344 medium. One cover slip was placed alongside the root, while another was positioned over the sample,
345 allowing gentle pressure to be applied by moving the first cover slip towards the root during imaging.
346 This setup was mounted onto the microscope stage and allowed to rest for 5 minutes for recovery.
347 During imaging, the inner cover slip was gradually pressed in until the root exhibited visible bending
348 (15-30°).

349 **ABA treatment**

350 ABA-induced stomatal closing was performed as follows. Lower epidermal cells were peeled from 7th
351 or 8th rosette leaf of 4-week-old *Arabidopsis*. The peeled epidermal cells were placed in buffer (30 mM
352 KCl, 10 mM MES, 50 µM CaCl2, pH 6.15) one night in advance and kept under plant growth condition
353 (150 µmol/s2/s, 16 hours light /8 hours dark) until the following day. After 3 hours into the circadian
354 lighting cycle, the stomata were allowed to open. 10 µM ABA was added in the buffer before starting
355 the imaging. Live stomatal images were captured using a Nikon Ti2E microscope with 40 x objective at
356 5 min/frame for 4 hours. The stomatal width was measure by Fiji software, with 10 stomata measured
357 per each treatment.

358 **Drought stress**

359 Young *Arabidopsis* seedlings grown on the 1/2MS plates were placed on the stage of Plants Axioplan 2
360 Zeiss Fluorescence Microscope. The lid was removed, reducing relative humidity from 100% to the

361 room humidity (~40%). Imaging was done for 30 minutes during which plants started to exhibit
362 stomatal Ca^{2+} transients. Whole leaves were imaged with ~480nm excitation and 500-550nm emission
363 filter.

364 **Molecular cloning and plant transformation**

365 Most of the plasmids generated in this study were generated using the Greengate system [37]. Greengate
366 building blocks were either obtained (source indicated in the primer list) or cloned using the Gibson
367 assembly (NEBuilder® HiFi DNA Assembly, NEB #E5520) of the backbone fragment and the insert
368 fragment. If BSAI sites were present, multiple fragments were used, and compatible cohesive ends
369 were used for mutagenesis.

pGGA-ARO2p	this study
pGGA-CNGC14p	this study
pGGA-UBQp	pGGA006 from [37]
pGGB-dummy	pGGB003 [37]
pGGB-GFP	pGGB004 [37]
pGG-B-6xHIS-C	Vector ID: 7_77; https://vectorvault.vib.be/
pGGC-ARO2 CDS	this study
pGGC-ARO2 CDS_stop	this study
pGGC-CNGC14 CDS	this study
pGGC-PBR	this study
pGGD-dummy	pGGD002 [37]
pGGD-linker-GFP	pGGD001 [37]
pGGD-linker-mCHERRY	pGGD003 [37]
pGGD-linker-mCITRINE	pGGD009 [37]
pGGD-mCITRINE	kindly provided by Andrea Bleckmann
pGGD-tID-HA	Vector ID: 12_40 ; https://vectorvault.vib.be/
pGGE – UBQ10 term.	pGGE009 [37]
pGGE- HSP18.2 term.	generously provied by Andrea Bleckmann
pGGF – HYG	pGGF005 [37]
pGGF-BASTA	pGGF001 [37]
pGGF-dALA	pGGF003 [37]
These blocks were combined in GoldenGate reactions as described in [37] in following combinations:	
CNGC14p:CNGC14-GFP	pGG-CNGC14p+pGGB-dummy+pGGC-CNGC14 CDS+pGGE UBQ10term+pGGF-dALA
UBQp:CNGC14-mCITRINE	pGGA-CNGC14p+pGGB-dummy+pGGC-CNGC14CDS+pGGD-linker-mCITRINE+pGGE-HSP18term+pGGF-BASTA
UBQp:CNGC2-mCITRINE	pGGA-UBQp+pGGB-dummy+pGGC-CNGC2 CDS+pGGD-mCITRINE+pGGE-UBQ10 term+pGGF-dALA
UBQp:ARO2-mCHERRY	pGGA-UBQp+pGGB-dummy+pGGC-ARO2 CDS+pGGD-linker-mCHERRY+pGGE-UBQ10 term+pGGF-dAla
UBQp:mCHERRY	pGGA-UBQp+pGGB-dummy+pGGC-dummy+pGGD-linker-mCHERRY+pGGE-UBQ10 term+pGGF-dAla

UBQp:6xHIS-ARO2	pGGA-UBQp+pGGB-6xHIS+pGGC-ARO2CDS_stop+pGGD-dummy+pGE-UBQ10term+pGGF-HIS
ARO2p:ARO2-mCIT	pGGA-ARO2p+pGGB-dummy+pGGC-ARO2CDS+pGGD-linkermCITRINE+pGE-HSP18t-+pGGF-HYG
ARO2p:GFP-PBR-tID-HA	pGGA-ARO2p+pGGB-GFP+pGGC-PBR+pGGD-tID-HA+pGGE-UBQ10term+pGGF-BASTA
ARO2p:ARO2-tID-HA	pGGA-ARO2p+pGGBdummy+pGGC-ARO2CDS+pGGE-tID-HA+pGGF-BASTA

Additional previously published plasmids were used NGR1-GFP from[38] CNGC14p:GFP-CNGC14 from[16], GFP-ROP2 from[15], CRK5 from[39] : These plasmids were then used for the "floral dip" agrobacterial transformation using *A. tumefaciens* strain GV3101[40]

Imaging and microfluidics

For the ARO-CNGC colocalization, vertical spinning disc microscope (vertical SD) Zeiss Axio Observer 7 coupled to a Yokogawa CSU-W1-T2 spinning disk unit with 50 µm pinholes and equipped with a VS-HOM1000 excitation light homogenizer (Visitron Systems), operated by the VisiView software (Visitron System) and with alpha Plan-Apochromat 100x/1.46, was used. The same microscope equipped with 5x/0.16 objective was used for observation of the root gravitropic bending (Supplementary movie 1) and for both the DII-Venus imaging and membrane depolarization assays, with Plan-Apochromat 20x/0.8 M27 obj.

For the Ca^{2+} measurements, vertical stage Zeiss LSM800 (vertical LSM) was used with air objective Plan Apochromat 10x/0.45 M27. GCaMP measurements were normalized by dividing 488nm-induced emission by 405nm induced emission, both between 500-550nm.

Microfluidic imaging was performed as introduced in[18]. This was used either for the membrane potential measurements[41] with vertical SD and Plan-Apochromat 20x/0.8 M27 with or for the treatments with individual elicitors and vertical LSM setup. For the mechanical bending experiments, Olympus X1000 confocal microscope with 10x dry objective was used. For the stomatal imaging, Axioplan 2 Zeiss Fluorescence Microscope was used.

FLIM imaging of *Nicotiana benth.* leaves

Transiently transformed *N. benthamiana* leaves with *A. tumefaciens* GV3101 (2 days post-transformation) were mounted on the glass slide and imaged, using Leica TCS SP8 FALCON microscope. HC PL APO 20x/0.75 CS objective was used for the imaging. The donor fluorophore was excited with 488 nm laser or 514nm laser, working in a pulsed mode with the 80 MHz frequency, and the signal was detected by HyD detector, working in Counting mode. Lifetime of the donor fluorophore was obtained from the Phasor Plot, built in LasX software (Leica Microsystems).

IP-MS

Lines expressing comparable amounts of ARO2-tID-HA and PBR-GFP-tID-HA were selected. 7-day old seedlings were homogenized using liquid nitrogen and immediately, extraction buffer was added (: 25 mM 2-amino-2-(hydroxymethyl)-1,3-propanediol hydrochloride (Tris–HCl) pH 7.8, 20 mM $MgCl_2$, 15 mM EDTA, 75 mM NaCl, 1 mM TCIP, 1 mM NaF, 0.5 mM $NaVO_3$, 15 mM β-glycerophosphate, 0.5 mM phenylmethanesulfonyl fluoride (PMSF), protease inhibitor cocktail, 0.1% Tween, 10% CHAPS. Mixture of buffer and powder 2:1 was then mixed for 1 hour at 4°C using a rotatory shaker and then centrifuged at 4°C and 20 min at 20 000x g. To the supernatant, 35ul of antiHA magnetic beads (Pierce Anti-HA

Magnetic Beads, Thermo Scientific; 88837) were added and incubated for 2 hours at 4°C while rotating. Then, 3 washes were done with IP buffer (same as extraction buffer, but lacking buffer protease inhibitors, PMSF, NaF, NaVO3, β -glycerophosphate, CHAPS). This was followed by 3 washes with the wash buffer (50 mM NaCl + 20 mM Tris). 5µL of the resulting beads were used for the quality check using SDS-PAGE and total protein visualizaiton. Resulting beads were subjected to the „on bead“ digest by trypisn and

All samples were processed using the iST kit (PreOmics GmbH) using the manufacturer's modified protocol for on-paramagnetic beads digest. Tryptic digestion was stopped after 1 h and cleaned-up samples were vacuum dried. Finally, samples were re-dissolved with 10 min sonication in the iST kit's LC LOAD buffer.

Raw files were searched in DiaNN version 1.8.1 in library-free mode against an *Arabidopsis thaliana* proteome sourced from UniprotKB. Match-Between-Runs was turned off. Fixed cysteine modification was set to Carbamidomethylation. Acetyl (protein N-term) was set as variable modification. Data was filtered at 1% FDR.

DiaNN's output was re-processed using in-house R scripts, starting from the main report table. Peptide-to-protein assignments were checked, then Protein Groups were assembled and quantified using an algorithm which: i) computes a mean protein group-level profile across samples using individual, normalized peptidoform profiles ("relative quantitation" step), then ii) following the best-flyer hypothesis, normalizes this profile to the mean intensity level of the most intense peptidoform ("unscaled absolute quantitation" step). Only unique and razor peptidoforms were used. Protein group-level quantitative values were normalized using the Levenberg-Marquardt procedure.

Expression in *Xenopus* oocytes and electrophysiology

cRNA preparation, oocyte injection and current recordings were performed as described (Chiasson et al. Elife 2017), with slight modifications. Following *in vitro* transcription (mMESSAGE mMACHINE™ T7 Transcription Kit, Invitrogen, Thermo Fischer), oocytes were injected with approximately 37 ng *CNGC14-VC,* and/or 13 ng *VN-ARO2* cRNA, and/or respective volumes of RNase-free water, using the Nanoject III (Drummond Scientific Company, Broomall, PA, USA). Injected oocytes were stored at 17°C in ND96 solution (96 mM NaCl, 2mM KCl, 1mM $CaCl_2$, 1 mM $MgCl_2$, 5 mM HEPES, pH 7.4/NaOH), supplemented with 25 µg/ml gentamycin for 2-3 days. For functional analysis, oocytes were constantly perfused with a bath solution containing 30 mM $CaCl_2$, 2 mM KCl, 10 mM MES-Tris pH7.4, and ion currents were studied by two-electrode voltage-clamp (TEVC), using the Turbo TEC-10CX amplifier (npi electronic GmbH, Tamm, Germany). Solutions were adjusted to 220 mosmol kg^{-1} using D-sorbitol. BiFC signals were imaged by confocal microscopy (Leica TCS SP5; Leica Microsystems, excitation: 514 nm, detection 520-556 nm.

Structural modeling

ARO2-CNGC14 complex was predicted via the Colabfold (version 1.5.2,[26]) implementation of AlphaFold2 (version multimer 3[25]). Any segment longer than 10 amino acids predicted with a pLDDT score below 50 was removed for the visualisation (Fig. 5) and further analysis. Additionally, residues 713 to 722 of CNGC14 flanked by long low-confident regions (pLDDT score below 50) were also removed. The truncated version of the ARO2-CNGC14 complex was positioned in the model plant plasma membrane using the PPM 3.0 Web Server (https://opm.phar.umich.edu/ppm_server3_cgopm, [42]).

Primers used in the study

pGGA-CNGC14p_rev	CGAGAATTCGGTCTCATGTTCTGTCACACCCATCAACC
pGGA-CNGC14p_for	GTGAAGCTTGGTCTCAACCTAAAAGACTTGAAATGGCCC
pGGA-CNGC2p_for	GTGAAGCTTGGTCTCAACCTCGATAAGTAAGTACATAAAATAATATTCC
pGGA-CNGC2p_rev	CGAGAATTCGGTCTCATGTTGGTGACTTGTTAGCTATAG

pGGA-backbone for	AACATGAGACCGAATTCTC
pGGA-backbone rev	AGGTTGAGACCAAGCTTC
pGGC-CNGC2CDS_for	GAAGCTTGGTCTCAGGCTCAATGCCCTCTCACCCCAAC
pGGC-CNGC2CDS_rev	CGAGAATTCGGTCTCACTGATTCGAGATGATCATGCGGTC
pGGC-CNGC14A_for	AAGCTTGGTCTCAGGCTCAATGATTCGTTTCTTGATCTTATTTTTTAAAC
pGGC-CNGC14A_rev	TCTCCTGGCCTCAGTGTGATTGAGTTG
pGGC-CNGC14B_for	TCACACTGAGGCCAGGAGATTTCTGTGGAG
pGGC-CNGC14B_rev	GAGAATTCGGTCTCACTGAATCATCCACTGAGAAATCC
pGGC-backbone for	TCAGTGAGACCGAATTCTCG
pGGC-backbone rev	TGAGCCTGAGACCAAGCTTC
pGGC-ARO2CDS_for	AGAAGTGAAGCTTGGTCTCAGGCTCCATGGCAGACATCGTCA
pGGC-ARO2CDS_rev	AGGGCGAGAATTCGGTCTCACTGAATTGAAATTGTAACCCCTTGATC
pGGC-ARO2CDS_rev2	GAGAATTCGGTCTCACTGATCAATTGAAATTGTAACCCC
pGGA-ARO2prom_for	AGAAGTGAAGCTTGGTCTCAACCTTATATACTAGAAGAGGAGTAAGTAA
pGGA-ARO2prom_rev	AGGGCGAGAATTCGGTCTCATGTTCGTCGATATCAGATCAAATGG
pGGC-PBRCDS_for	TATTCTTCTTCTTCTTCTTCTGCTTCATGGAGCCTGAGACCAAGCTTCACTTCT
pGGC-PBRCDS_rev	AGAAGAAGAAGAAGAATAAGAACCGTTCAGTGAGACCGAATTCTCGCCCT
pGGC_cngc14_m1_for	CTTGTGCAGTACAAGTCGCTTGGGCGCGGTATAAGAGAAAGAAGTTGGC
pGGC_cngc14_m1_rev	CTTGTACTGCACAAGCAGCCCAAGTCGCCCACTGATGGGAGTAATAACGG
pGGC_ARO2_m1_for	GCAGATTGCCATTCTCGTCACCGGATCGCTTGAAGACCGCTCT
pGGC_ARO2_m1_rev	CGAACCCATCCTTTGCCTGATCTGGCGGCAGATTGCCATTCTCG
pGGC_ARO2_m3_rev	AGCCAGCCTTACCACGGTCTTCCGCCGGAGCGGCGAC
pGGC_ARO2_m3_for	GTGGTAAGGCTGGCTACCTTGGTCTTCCACCAATCGCC

Acknowledgements

This project was supported by the Czech Science Foundation grant Nr. 25-16449S and by European Union, Horizon Europe, project MOLIPEC, ID 101087030. Computational resources used for structural modeling were provided by the e-INFRA CZ project (ID:90254), supported by the Ministry of Education, Youth and Sports of the Czech Republic. Part of the work was carried out with the support of a Growth Facility (BC Core Facilities; IPMB BC CAS). X. laevis oocytes were kindly provided by C. Korbmacher on a regular basis (FAU Erlangen-Nürnberg). MF received support from the European Research Council (Grant 480 No. 101125499). We acknowledge the core facility LMH, the BC CAS supported by the MEYS CR (LM 2023050 Czech-BioImaging). DO received support from the Czech Science Foundation grant Nr. 24-12107S

References

1. Tan, Y.-Q. *et al.* Multiple cyclic nucleotide-gated channels function as ABA-activated Ca2+ channels required for ABA-induced stomatal closure in Arabidopsis. *The Plant Cell* **35**, 239–259 (2023).
2. Yang, Y. *et al.* OPEN STOMATA 1 phosphorylates CYCLIC NUCLEOTIDE-GATED CHANNELs to trigger Ca2+ signaling for abscisic acid-induced stomatal closure in Arabidopsis. *The Plant Cell* koae073 (2024) doi:10.1093/plcell/koae073.
3. Brost, C. *et al.* Multiple cyclic nucleotide-gated channels coordinate calcium oscillations and polar growth of root hairs. *The Plant Journal* **99**, 910–923 (2019).

4. Gao, Q.-F. *et al.* Cyclic nucleotide-gated channel 18 is an essential Ca2+ channel in pollen tube tips for pollen tube guidance to ovules in Arabidopsis. *Proceedings of the National Academy of Sciences* **113**, 3096–3101 (2016).
5. Ma, Y., Garrido, K., Ali, R. & Berkowitz, G. A. Phenotypes of cyclic nucleotide-gated cation channel mutants: probing the nature of native channels. *The Plant Journal* **113**, 1223–1236 (2023).
6. Qi, Z. *et al.* Ca2+ signaling by plant Arabidopsis thaliana Pep peptides depends on AtPepR1, a receptor with guanylyl cyclase activity, and cGMP-activated Ca2+ channels. *Proceedings of the National Academy of Sciences* **107**, 21193–21198 (2010).
7. Wang, L. *et al.* Arabidopsis thaliana CYCLIC NUCLEOTIDE-GATED CHANNEL2 mediates extracellular ATP signal transduction in root epidermis. *New Phytologist* **234**, 412–421 (2022).
8. Shih, H.-W., DePew, C. L., Miller, N. D. & Monshausen, G. B. The Cyclic Nucleotide-Gated Channel CNGC14 Regulates Root Gravitropism in Arabidopsis thaliana. *Current Biology* **25**, 3119–3125 (2015).
9. Balagué, C. *et al.* HLM1, an Essential Signaling Component in the Hypersensitive Response, Is a Member of the Cyclic Nucleotide–Gated Channel Ion Channel Family. *Plant Cell* **15**, 365–379 (2003).
10. Jarratt-Barnham, E., Wang, L., Ning, Y. & Davies, J. M. The Complex Story of Plant Cyclic Nucleotide-Gated Channels. *Int J Mol Sci* **22**, 874 (2021).
11. Leng, Q., Mercier, R. W., Hua, B.-G., Fromm, H. & Berkowitz, G. A. Electrophysiological Analysis of Cloned Cyclic Nucleotide-Gated Ion Channels. *Plant Physiology* **128**, 400–410 (2002).
12. Tian, W. *et al.* A calmodulin-gated calcium channel links pathogen patterns to plant immunity. *Nature* **572**, 131–135 (2019).
13. Curran, A. *et al.* Calcium-dependent protein kinases from Arabidopsis show substrate specificity differences in an analysis of 103 substrates. *Front Plant Sci* **2**, 36 (2011).
14. Gebert, M., Dresselhaus, T. & Sprunck, S. F-Actin Organization and Pollen Tube Tip Growth in *Arabidopsis* Are Dependent on the Gametophyte-Specific Armadillo Repeat Protein ARO1. *The Plant Cell* **20**, 2798–2814 (2008).
15. Kulich, I. *et al.* ARMADILLO REPEAT ONLY proteins confine Rho GTPase signalling to polar growth sites. *Nat Plants* **6**, 1275–1288 (2020).
16. Serre, N. B. *et al.* The AUX1-AFB1-CNGC14 module establishes a longitudinal root surface pH profile. *eLife* **12**, e85193 (2023).
17. Dubey, S. M. *et al.* The AFB1 auxin receptor controls the cytoplasmic auxin response pathway in Arabidopsis thaliana. *Molecular Plant* **16**, 1120–1130 (2023).
18. Serre, N. B. C. *et al.* AFB1 controls rapid auxin signalling through membrane depolarization in Arabidopsis thaliana root. *Nat. Plants* **7**, 1229–1238 (2021).
19. Prigge, M. J. *et al.* Genetic analysis of the Arabidopsis TIR1/AFB auxin receptors reveals both overlapping and specialized functions. *eLife* **9**, e54740 (2020).
20. Chen, H., Li, L., Zou, M., Qi, L. & Friml, J. Distinct functions of TIR1 and AFB1 receptors in auxin signaling. *Molecular Plant* **16**, 1117–1119 (2023).
21. Fendrych, M. *et al.* Rapid and reversible root growth inhibition by TIR1 auxin signalling. *Nature Plants* **4**, 453–459 (2018).
22. Toyota, M. *et al.* Glutamate triggers long-distance, calcium-based plant defense signaling. *Science* **361**, 1112–1115 (2018).
23. Duong, H. N. *et al.* Cyclic nucleotide-gated ion channel 6 is involved in extracellular ATP signaling and plant immunity. *The Plant Journal* **109**, 1386–1396 (2022).
24. Yoshimura, K., Iida, K. & Iida, H. MCAs in Arabidopsis are Ca2+-permeable mechanosensitive channels inherently sensitive to membrane tension. *Nat Commun* **12**, 6074 (2021).
25. Jumper, J. *et al.* Highly accurate protein structure prediction with AlphaFold. *Nature* **596**, 583–589 (2021).
26. Mirdita, M. *et al.* ColabFold: making protein folding accessible to all. *Nat Methods* **19**, 679–682 (2022).

27. Fischer, C. *et al.* Calmodulin as a Ca2+-Sensing Subunit of Arabidopsis Cyclic Nucleotide-Gated Channel Complexes. *Plant and Cell Physiology* **58**, 1208–1221 (2017).
28. Dietrich, P., Moeder, W. & Yoshioka, K. Plant Cyclic Nucleotide-Gated Channels: New Insights on Their Functions and Regulation1[OPEN]. *Plant Physiol* **184**, 27–38 (2020).
29. Clough, S. J. *et al.* The Arabidopsis dnd1 “defense, no death” gene encodes a mutated cyclic nucleotide-gated ion channel. *Proceedings of the National Academy of Sciences* **97**, 9323–9328 (2000).
30. Jurkowski, G. I. *et al.* Arabidopsis DND2, a Second Cyclic Nucleotide-Gated Ion Channel Gene for Which Mutation Causes the “Defense, No Death” Phenotype. *MPMI* **17**, 511–520 (2004).
31. Hwang, J.-U., Vernoud, V., Szumlanski, A., Nielsen, E. & Yang, Z. A Tip-Localized RhoGAP Controls Cell Polarity by Globally Inhibiting Rho GTPase at the Cell Apex. *Current Biology* **18**, 1907–1916 (2008).
32. Cárdenas, L., Lovy-Wheeler, A., Kunkel, J. G. & Hepler, P. K. Pollen Tube Growth Oscillations and Intracellular Calcium Levels Are Reversibly Modulated by Actin Polymerization. *Plant Physiology* **146**, 1611–1621 (2008).
33. Fischer, C., Kugler, A., Hoth, S. & Dietrich, P. An IQ Domain Mediates the Interaction with Calmodulin in a Plant Cyclic Nucleotide-Gated Channel. *Plant and Cell Physiology* **54**, 573–584 (2013).
34. Weiss, N. & Zamponi, G. W. The T-type calcium channelosome. *Pflugers Arch - Eur J Physiol* **476**, 163–177 (2024).
35. Liao, C.-Y. *et al.* Reporters for sensitive and quantitative measurement of auxin response. *Nat Methods* **12**, 207–210 (2015).
36. Schindelin, J. *et al.* Fiji: an open-source platform for biological-image analysis. *Nat Methods* **9**, 676–682 (2012).
37. Lampropoulos, A. *et al.* GreenGate - A Novel, Versatile, and Efficient Cloning System for Plant Transgenesis. *PLOS ONE* **8**, e83043 (2013).
38. Kulich, I., Schmid, J., Teplova, A., Qi, L. & Friml, J. Rapid translocation of NGR proteins driving polarization of PIN-activating D6 protein kinase during root gravitropism. *eLife* **12**, RP91523 (2024).
39. Rigó, G. *et al.* Inactivation of plasma membrane-localized CDPK-RELATED KINASE5 decelerates PIN2 exocytosis and root gravitropic response in Arabidopsis. *Plant Cell* **25**, 1592–1608 (2013).
40. Clough, S. J. & Bent, A. F. Floral dip: a simplified method for -mediated transformation of. *The Plant Journal* **16**, 735–743 (1998).
41. Dubey, S., Fendrych, M. & Serre, N. Relative Membrane Potential Measurements Using $DISBAC_2(3)$ Fluorescence in Arabidopsis thaliana Primary Roots. *BIO-PROTOCOL* **13**, (2023).
42. Lomize, A. L., Todd, S. C. & Pogozheva, I. D. Spatial arrangement of proteins in planar and curved membranes by PPM 3.0. *Protein Sci* **31**, 209–220 (2022).